Multi doped Hydroxyapatite-Urea Nano fertilizer: Synthesis and Controlled Micronutrient Release

Ezekiel Iliya

Department of Ceramic Technology, School of Applied Science and Technology, Auchi Polytechnic Auchi P.M.B 13 Edo State, Nigeria.
*Corresponding author email: Email: eiliya@auchiploy.edu.ng; +2348062682465

Direct Research Journal of Engineering and Information Technology

Vol. 14(1), Pp. 1-11, January 2026,

Research Article
ISSN: 2354-4155
https://journals.directresearchpublisher.org/index.php/drjeit; https://www.ajol.info/index.php/drjeit

Received 5 December 2025, Accepted 10 January 2026, Published 14 January 2026

ABSTRACT

Hydroxyapatite HAp-urea composite based nano fertilizer constitutes a novel approach of incorporating variety of ionic species into HAp hexagonal lattice structure with control release capabilities. Evidently, it is a veritable and sustainable alternative to commercial fertilizer in enhancing plant yield in nutrient deficient soil. In this research, HAp doped with multi ionic species of Mg2+, Si4+ and Cu2+ (Ca10-w/2-x-ySiw+MgxCuy(PO4)6-w(OH)2-w) with nutrient and subsequently form a HAp-urea nano fertilizer composite via chemical precipitation route. The following HAp to nano-urea matrix-filler ratio 100 mL: 0.15 g was adopted. The crystallinity, chemical constituent and nanoparticle sizes was investigated using X-ray diffractometry (XRD), X-ray fluorescence (XRF), Transmission Electron Microscope (TEM), Brunauer–Emmett–Teller (BET) and Scanning Electron Microscopy (SEM). Micronutrient ion release of Ca2+, P5+, Mg2+ and Cu2+ was examined using Inductively Coupled Plasma Optical Emission Spectroscopy (ICP-OES) in water sample and XRF in soil sample. Monitored plant foliage activities was analyzed by applying 10g of the produced HAp-urea nanofertilizer composite in comparison to 10g of commercial fertilizer on selected plants. Ultimately, the multidoped HAp-urea composite based nanofertilizer showed superior plant growth height (PGH) of HU: 54, HUMS: 58 and HUMSC: 56 cm as compared to commercial fertilizer with PGH of 36 cm.

Keywords: *Hydroxyapatite, urea, nanofertilizer, controlled release, nanocomposite, sustainable agriculture, ICP-OES*

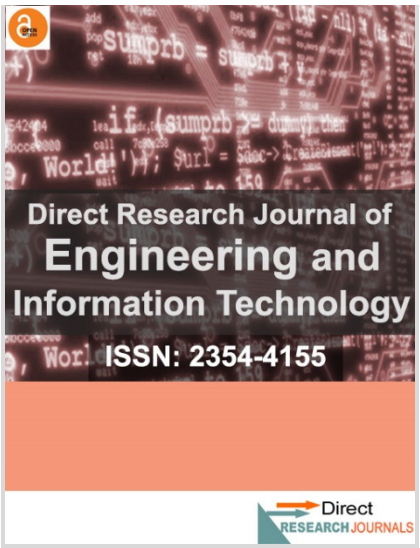

Citation: Iliya, E. (2026). Multi doped Hydroxyapatite-Urea Nano fertilizer: Synthesis and Controlled Micronutrient Release. *Direct Research Journal of Engineering and Information Technology*, 14(1), Pp. 1-11. https://doi.org/10.26765/DRJEIT14235180

INTRODUCTION

Climate change's effects on agricultural productivity and food security have emerged as a major worldwide problem, attracting significant attention and discussion. Climate change is widely considered to be mostly caused by human actions such as land use changes, deforestation, excessive fertilizer application, and fossil fuel burning (Kabato, Getnet, Sinore, Nemeth, and Molnár, 2025). Climate-smart agriculture (C-SA) has developed as a holistic solution to the triple issue of boosting agricultural productivity while adapting to climate change and reducing greenhouse gas emissions. Globally, C-SA implementation can enhance crop yields by 10-23%, improve water usage efficiency by 20-40%, and minimize production risks by 15-30% when compared to traditional farming approaches. Using C-SA in sub-Saharan Africa reduces crop failure rates by 40-60% during droughts and accelerates post-disaster recovery periods by 30-50% when compared to traditional systems (Aziz, Majid, Peters, Amanullah, Md, Hafeez, Sirilak, Khalid, Habibullah, and Shakeel, 2026). The combination of nanofertilizers and climate-smart agriculture (C-SA) methods is a possible

avenue for attaining long-term soil, water, and environmental management in the face of changing climatic conditions (Imran and Hayat, 2025). Remote sensing and modeling advances have enabled exact monitoring of soil moisture and temperature dynamics, which is crucial for optimizing nano fertilizer delivery and improving soil-water interactions (Wei, Kou, Miao, Hu, Li, Wu, and Meng, 2025; Wu and Zhao 2024). Similarly, climatic models and isotopic records offer useful insights into hydrological cycles and surface water stability, allowing for more efficient irrigation and nutrient management (Li, Zhu, Chen, Qi, Lu, Meng, and Gun, 2025; Zhang and Wu, 2025). There are two ways to create nanofertilizers: top-down synthesis, which uses physical and biological synthesis, and bottom-up synthesis, which uses chemical synthesis. Self-assembly and self-organization are used in bottom-up nanotechnology to create materials at the nanoscale. According to Ashraf, Batool, Ghaffar, Imran, Riaz, Hussaan, Farooq, and Rasul (2025), nanoscale fertilizer promotes soil biological health, mobilizes soil nutrients, and produces high-production, nutritious food while conserving natural resources. Commercially available phosphorus fertilizers commonly have low efficiencies due to their immobilization in soil, and a large part of these fertilizers are not plant-available. Besides, phosphorus resources are non-renewable (Liu et al.,2017). Recently, a significant amount of attention has been focus on nanofertilizers due to their slow or controlled release and also their very lesser particle size which increases the solubility and uptake of nanoparticles in plant. Hydroxyapatite nanoparticles are of great prominence as phosphorus nanofertilizer due to their very low toxicity, biocompatibility, and the fact that products obtained from their degradation, i.e., phosphate and calcium ions, are naturally available in soils (Noruzi, Hadian, Soleimanpour, Ma'mani, and Shahbazi, 2023).

In contemporary agriculture, HAp has the potential to be a very effective phosphorus fertilizer. Its naturally rich content of vital macronutrients, such as calcium (Ca^{2+}) and phosphorus (P^{5+}), which are required for plant growth and development, is one of its remarkable characteristics. These nutrients are readily available within apatite, giving plants a useful and convenient source of nourishment that promotes healthy growth and higher yields (Wang, Jin, & Jaisi, 2015). Furthermore, because HAp is biocompatible, it is frequently a safe option for agricultural use (Thathsarani, 2021; Carmona, Guagliardi, and Masciocchi, 2022). Its biocompatibility increases its potential for sustainable and ecologically friendly farming practices. The particle size of HAp greatly enhances its fertilizer efficacy if it attains a high surface-to-volume ratio (Usman, Farooq, Wakeel, Nawaz, Cheema, Rehman, Ashraf, and Sanaullah, 2020; Sajadinia, Ghazanfari, Naghavii, Naghavi, and Tahamipur, 2021). It has been established that the particle size of HAp is significant due to the possibility of toxicity and must be accurately controlled before widespread application is permitted (Rao, Sun, and Ouyang, 2019).

Furthermore, HAp's pH-responsive solubility sets it apart from typical P fertilizers (Huang, Wu, Li, Cheng, He, Tian, and Huang, 2016; Samadi, Pourmadadi, Yazdian, Rashedi, and Navaei-Nigjeh, 2021). Because of this property, HAp may respond fast to pH changes in the soil, releasing calcium and phosphate ions only when the plants require them. The delayed and targeted release of nutrients corresponds to the stages of crop growth preventing nutrient waste and leaching. As a result, higher nutrient uptake efficiency increases crop health and resilience, which contributes to greater agricultural sustainability. Sajadinia et al. studied the effects of four different fertilizers on the growth parameters of Zea mays L. Among these, HAp fertilizers had the greatest impact on maize growth. In comparison to traditional commercial fertilizers such as simple and triple superphosphate (SSP and TSP), HAp-based fertilizers were more successful at improving maize characteristics. HAP increased maize height by 50% compared to SSP and control, and 36% compared to TSP (Sajadinia et al, 2021).

Finally, HAp provides a large surface area for interaction with other nutrient-containing molecules. This feature allows for effective adsorption of critical elements onto its surface, promoting controlled nutrient release and uptake by plants throughout time (Fuad, Ang, Nabil, and Shuhaime, 2023). Another feature of HAp is its adaptability to cation or anion doping, which allows for the customization of its properties to specific agricultural applications (Sharma, Shrivastava, Afonso, Soni, and Cahill, 2022; Ammar, S. Ashraf, and J. Baltrusaitis, 2023). This adaptability allows researchers to create fertilizer properties depending on HAp, such as nutrient release rates and compatibility with various soil types and crops, for optimal agronomic results. One rapidly expanding topic is the formulation of N-P-(Ca) fertilizer products that use HAp to stabilize urea and reduce nitrogen release rates (Ammar, M., Ashraf, S., & Jonas Baltrusaitis, 2025). Synthetic hydroxyapatite is the most often utilized bioresorbable material; however β-TCP and bisphosphate are equally effective in tissue repair and replacement. Hydroxyapatite has been demonstrated to contain significant amounts of ion substitution, including ions required for plant growth (Siracusa, Maimone, and Antonelli, 2021). In general, small properties, such as nanoscale size and homogeneity, can be efficiently combined using synthesis methods such as wet chemical procedures. Co-precipitation is considered as a simplified approach for creating nanoparticles with complementary bioresorption capabilities, using only basic equipment (Dawar, Chitkara, Sandhu, Jolly, and Malhotra, 2016). In contrast, employing fertilizers such as HAp-Urea nanofertilizer results in a slow and sustainable release of nutrients, this improves nutrient use. The capacity of HAp-Urea nanofertilizer to distribute nutrients slowly and sustainably improves plant nitrogen agronomic efficiency while slowing urea decomposition in soil. Furthermore, micronutrients such as Ca^{2+}, P^{5+}, Mg^{2+} and Cu^{2+}, which are essential for plant growth, can be integrated into the lattice

structure of HAp. A HAp-Urea nanofertilizer composite will allow for more effective nutrient uptake due to nanofertilization and the presence of numerous ionic replacements, which are completely absent in conventional fertilizers (Carmona et al., 2021).

The essential minerals in soil include phosphorus (P), potassium (K), magnesium (Mg), calcium (Ca), sulfur (S), and micronutrients such as molybdenum (Mo), boron (B), zinc (Zn), copper (Cu), and iron (Fe), which are irregularly distributed among countries. Correlation studies indicate that soil qualities and the prevalence of nutrient deficiencies are related to the limited availability of both essential nutrients and micronutrient ions. Nutrient restrictions have been reported to vary between soils, both within specific countries and across the African continent. Potassium, phosphorus, magnesium, and sulfur are particularly lacking nutrients. There are substantial nutrient deficits in Nigeria, particularly in phosphorus, zinc, and magnesium (Baijukya, 2021). To overcome these shortages, fertilizers containing enough amounts of both essential nutrients and micronutrients have been advised. Commercial fertilizers have been widely used for more than 50 years due to their balanced composition of the three basic nutrients: nitrogen (N), phosphorus (P), and potassium. These three critical nutrients are required for proper plant growth and development. The most often used commercial fertilizers include SSP, TSP, urea, NPK, MAP, and DAP. These fertilizers offer plants with critical minerals, including nitrogen, potassium, and phosphorus (Lubkowski, 2016).

Hydroxyapatite (HAp) has been recognized as a good source of phosphorus fertilizer. HAp, a key mineral for hard tissues, is a well-known biomaterial that has been studied for a variety of biomedical applications, including tissue engineering, dental implants, and bone grafting. Furthermore, the nano-engineered variant of HAp has already been identified as an effective fertilizer in laboratory conditions. Hydroxyapatite has been demonstrated to provide appropriate phosphorus nutrients to crops. In contrast to soluble phosphate PO_4^{3-}salts and solid PO_4^{3-}, HAp has restricted mobility to neighboring agricultural areas, suggesting a substantial potential for increasing agricultural production (Tarafder, Daizy, Alam, Ali, Islam, Islam, Ahommed, Aly, and Khan, 2020). Several methods for producing hydroxyapatite have been documented, including wet chemical deposition, biomimetic approaches, sol-gel techniques, and hydrothermal procedures (Ayushi, Ratul, Aaron, and Pushplata, 2019).

Urea molecules can bind to the surface of HAp particles, perhaps resulting in decreased N solubility, albeit the precise binding or delayed N release process is unknown (Fernan et al., 2020). Kottegoda et al. (2017) produced HAp/urea at a weight ratio of 6:1. In column dissolution studies, they discovered that HAP/urea released equal N amounts 12 times slower than pure urea. Furthermore, HAp/urea was linked to higher rice crop yields at 50% reduced applied nitrogen content. It was postulated as a result of urea-HAp interaction via amine and carbonyl groups (Kottegoda, Sandaruwan, Priyadarshana, Siriwardhana, Rathnayake, Arachchige, Kumarasinghe, Dahanayake, Karunaratne, and Amaratunga, 2017). Similarly, Pohshna et al. generated HAP/urea materials with a weight ratio of 5:1 and referred to them as urea-doped HAp nanomaterials, despite the fact that their experimental processes were sol-gel at low temperatures, which is unlikely to result in doping. The use of these materials in rice fertilization with N60: P175: K50 or a half-recommended dose of N120: P60: K50 resulted in comparable biomass yields and plant height. The results also showed a high efficacy of N utilization (76%) and P (14%), indicating a significant reduction in nutrient leaching. While not complete, their findings suggest that hybrid HAp/urea materials have the ability to produce biomass growth performance indicators while utilizing half the nitrogen of solo urea (Pohshna and D. R. Mailapalli, 2021).

The use of HAp as a stabilizing agent to reduce nitrogen release is an intriguing idea. Recent studies have shown that HAP nanorods can reduce the release rate of complexed urea by up to 11.5 times that of pure urea (Maghsoodi, Najaf, Reyhanitabar, and Oustan, 2020). They discovered that pure urea dissolved fully in deionized water after 40 seconds, whereas HAp/urea released around 90% of the urea after 480 seconds.38 Kottegoda et al. (2017) discovered that HAp/urea released N at a more than 12-fold slower rate than pure urea, which is consistent with the findings of Maghsoodi et al. (2020). In particular, in these trials, almost 99% of N was released in urea after 5 minutes, whereas around 86% was released in water after 1 hour and the remaining 14% after a week. Tarafder et al. (2020) demonstrated that HAp/urea had a slow nutrient release rate in both soil and water, albeit the reasons for the slower nutrient release in water were not evident. After 14 days, urea-modified HAp particles released around 0.1% and 1% of NO^{2-} into water and soil, respectively. After 14 days, the emission of PO_4^{3-} was 1% in soil and 6% in water. Interestingly, the authors found approximately 320% NO^{3-} release in the soil after 14 days, but did not elaborate on the apparent nitrogen balance increase. Finally, investigations revealed that the HAp/urea/montmorillonite combination released N at substantially slower rates than pure urea. In particular, in the soil column, urea released around 70% of its nitrogen after 30 days, whereas HAp/urea/montmorillonite released the same amount 20 days later. As a result, kinetic release patterns of hybrid HAp/urea materials are reported to differ from those of pure urea, and nutrient release patterns reported thus far paint a complex picture with implications for strongly inhibited urea dissolution from HAp/urea materials (Madusanka et al., 2017; Fernando et a., 2021). The crystal structure investigation is critical in improving our understanding of urea-HAp interactions. Interactions between dissimilar materials have the ability to create voids, structural flaws, and distortion. As a result, identifying plane shifts or intensity variations can reveal the

governing dynamics that underlie these changes. Pure urea has discrete peaks at 22.25°, 29.32°, 24.62°, 35.53°, and 37.12°, which correspond to Miller indices of (110), (111), (101), (210), and (201), respectively (Elshay, Nada, Farroh, AL-Huqail, Aljabri, Binothman and Seleiman, 2022). Notably, the most prominent peak corresponds to the (110) plane. On the other hand, HAp has two primary types of crystal structures: hexagonal and monoclinic.

Hexagonal crystal symmetry is the most popular in agricultural applications. The hexagonal symmetry is a part of a hexagonal unit cell and the P63/m space group. According to Fihri, Len, Varma, and Solhy (2017), the crystallographic parameters of a and c are 9.418 and 6.881 Å, respectively. HAp in the urea-containing chemical material can have a variety of crystallinities, ranging from amorphous to highly crystalline bulk. The conditions of the synthesis technique are the main determinant of this. In another study, HAp was synthesized chemically, and both urea and HAp were produced in a well-dispersed solution. The hexagonal symmetry of HAp was shown by the XRD investigation. The existence of urea was detected using its tetragonal symmetry and, after washing, the urea was still detected by XRD. This demonstrated the robust adhesion of urea and HAp within the hybrid material. The HAp structure remained unchanged as a result of this urea addition impregnation procedure (Elhassani, Essamlali, Aqlil, Nzenguet, Ganetri, and Zahouily, 2019). In a research by Sharma et al., urea showed notable peaks for (hkl) planes of (210), (111), and (110). These planes shifted due to structural alterations and rearrangements (Sharma et al., 2022). Some summits disappeared, including the peak in the (110) plane. As a result, the inclusion of urea on the HAp surface can cause a change in urea structure. The preparation of Elhassani's and Sharma's works differed in temperature. Sharma et al. employed 50 °C for HAp production and combination with urea. However, Abeywardana et al. produced HAP/urea composites and found no peak shifts in HAp (hexagonal structure) after adding urea (Abeywardana, de Silva, Sandaruwan, Dahanayake, Priyadarshana, Chathurika, Karunaratne, and Kottegoda, 2021). There was no increase in temperature during the preparation. As a result, higher temperatures during the urea-HAp mixing stage may cause structural changes in urea.

Other nutrients were also included into the HAP/urea hybrid composites. Zn-HAP/urea composites increased plant height and dry weight. Other experiments revealed that urea had lower intensity peaks, indicating a probable disturbance of the crystal structure due to contact with HAp Tarafder et al., (2020). They attributed this impact to the metal-ligand interaction of N and Ca atoms in newly generated HAp/urea composites. They also demonstrated that treating A. esculentus plants with a low weekly dose (50 mg) of Cu-Fe-Zn-HAP/urea fertilizer resulted in a statistically significant increase in nitrogen usage efficiency. Ram'ırez Rodr'ıguez et al. found that incorporating urea into amorphous calcium phosphate reduced the intense peak at 22° to an amorphous pattern with a broad peak at 32.5° (Ram'ırez-Rodr'ıguez et al.). This means that urea can be incorporated into the hybrid HAp/urea material as a single phase, as long as the concentrations allow for excess urea, which causes phase segregation. As a result, several HAp/urea composites with high urea content showed crystalline morphologies similar to the segregated parent compounds (Kottegoda et al., 2017). Sharma et al. (2022) investigated the effect of Zn/Mg doped HAp/urea on wheat growth and utilization. The findings revealed that elemental dopants can be utilized to control the crystallinity of HAp, and hence its nitrogen loading capability. Furthermore, utilizing 50% and 25% of Zn/Mg-HAp/urea resulted in wheat growth comparable to 100% urea dosages. Notably, HAp or HAp/urea hybrids did not exhibit the normal crystalline pattern of HAp, making it impossible to identify the peak shift of urea in the HAp structure after doping Mg and Zn.

Several studies on the leaching of the HAp and urea composite show a regulated release of nutrients such Ca^{2+}, PO_4^{3-}, NO^{2-}, NO^{3-}, Cu^{2+}, Mg^{2+}, and Zn^{2+}. Additionally, Cu^{2+}, Fe^{2+}, and Zn^{2+} nutrients were detected by inductively coupled plasma-optical emission spectrometry (ICP-OES) (Baijukya, 2021). Other important characterization techniques used include X-ray fluorescence (XRF), X-ray diffractometry (XRD), Transmission Electron Microscopy (TEM), Brunauer-Emmett-Teller (BET) analysis, and scanning electron microscopy (SEM).

Therefore, the goal of this study is to synthesize a multidoped HAp-Urea nanofertilizer composite, assess micronutrient release, and perform plant growth/foliar activities on a sampled plant. The study unveils comparative performance of nanocomposite samples against commercial fertilizers and the mechanistic insights into nutrient release of the entire nanocomposite. In addition, the HAp-Urea nanofertilizer composite was characterized using XRF, XRD, FESEM, FTIR, BET, TEM, and ICP- OES protocol.

MATERIALS AND METHODS

Materials for HAp-Urea Nanofertilizer

Ultrafine Calcium carbonate ($CaCO_3$) from Ikpeshi Edo State, Nigeria in combination with laboratory grade H_3PO_4 (Merck) was selected as sources of $Ca^{2+}$and PO_4^{3-}, respectively. Nitrate compounds (all Merck) of Mg^{2+} and Cu^{2+} provide the ionic dopants in the HAp lattice structur,e. Other important solvents to be used include sodium hydroxide (NaOH) and deionised water (H_2O). Deionised water serves as dissolution solvents and NaOH acts as pH regulator. Trisodium citrate ($Na_3C_6H_5O_7$) and Urea molecules ($CO(NH_2)_2$) was use to prepare the nano-urea.

Synthesis of Multidoped HAp Nanoparticles

The multidopeded HAp was prepared using wet chemical route in accordance to Eq. (1), (2) and (3). The ultrafine

Table 1: Summary of acronyms and phase formula use in synthesis

Acronym	Crystal Phase formulation	Eq.
HU	$[Ca_{10}(PO_4)_6(OH)_{2.00}]$ + Urea	(4.0)
HUMS	$[Ca_{9.220}Mg_{0.760}(PO_4)_{5.922}(SiO_4)_{0.0371}(OH)_{1.963}]$ + Urea	(5.0)
HUMSC	$[Ca_{9.220}Mg_{0.760}Cu_{0.0001}(PO_4)_{5.923}(SiO_4)_{0.0371}(OH)_{1.963}]$ + Urea	(6.0)

$CaCO_3$ was calcined at 600°C and the resultant calcite co-precipitated with orthophosphate solution at 80 °C for 5 Hrs. Each dopant was introduced into the solution as the synthesis commences. The solid mass obtained from the reactants is then dried at 100 °C for 24 Hrs in an oven. The synthesized multidoped HAp naoparticles was manually milled using pestle and agate mortar. The milled HAp nanoparticle will then be milled using 100 µm sieves.

$$CaCO_3 \rightarrow CaO + CO_2 \text{ (calcined at 600°C)} \quad (1)$$

$$10CaO + 6H_3PO_4 \rightarrow Ca_{10}(PO4)_6(OH)_2 + 8H_2O \quad (2)$$

$$Ca_{10-w/2-x-y}(PO_4)_{6-w}(OH)_2 + wSi^{4+} + xMg^{2+} + yCu^{2+} \rightarrow Ca10_{-w/2-x-y}Si_w + Mg_xCu_y(PO_4)_{6-w}(OH)_{2-w} \quad (3)$$

Synthesis of Urea

Nano-urea was prepared by mixing urea molecules and trisodium citrate under optimum conditions. First, 0.30 g of urea molecules was mixed with 0.86 g of trisodium citrate in a beaker. The mixture will then be heated gradually up to 90 °C for 1 h using a hot plate. Trisodium citrate functions as nitrification inhibitor for nanourea production. After heating process, the color of the solution should become ash, indicating the presence of nano-urea.

Preparation of HAp-Urea nanofertilizers

Three treated suspension of 100 mL HAp and 100 mL multidoped HAp was each mixed with 0.15 g of synthesized nano-urea. The dispersion was prepared under ultrasound sonication (30 kHz for 1 h). Moreover, the mixture was allowed to settle, and the excess liquid was drained off. The resulting mixture was further centrifuged and washed three times with distilled water. Finally, nano-urea/ multidoped HAp nanoparticles was dried at 100 °C for 24 h and finely powdered with a hand mortar. The powder was characterized using SEM, X-ray diffraction (XRD), and Fourier-transform infrared spectroscopy (FTIR). The compositions HAp-Urea, Mg-Si doped HAp-Urea and Mg-Si-Cu doped HAp-Urea are hereinafter named; HU, HUMS and HUMSC as shown in (Table 1). In Table 1, formation of HAp-nanourea composite formulation is established by matrix of HAp:

10CaO + 6H3PO4 → Ca10 (PO4)6(OH) 2 + 8H2O from Eq. (2) and filler of urea to form HU ([Ca10 (PO4)6(OH) 2.00] + Urea) as Eq. (4). Similarly, multidoped HAp-nanourea composite formulation is prepared by matrix of multidoped HAp: Ca10-w/2−x−y(PO4)6-w(OH)2 + wSi4+ + xMg2+ + yCu2+ → w/2-x-y Siw+MgxCuy(PO4)6-w(OH)2-w from Eq. (3) and filler of urea to form HUMS ([Ca9.220Mg0.760(PO4)5.922(SiO4)0.0371(OH)1.963] + Urea) as Eq. (5) and HUMSC ([Ca9.220Mg0.760Cu0.0001(PO4)5.923(SiO4)0.0371(OH)1.963] + Urea) as Eq.(6).

Characterization of HAp-Urea nanofertilizers

HAp-Urea nanofertilizer characterization will engage the use of X-ray diffractometry (XRD), X-ray fluorescence (XRF), Transmission Electron Microscope (TEM),*Brunauer–Emmett–Teller* (BET), using Inductively Coupled Plasma Optical Emission Spectroscopy (ICP-OES) and Scanning Electron Microscopy (SEM) for investigating crystallinity, chemical constituent, particle sizes and morphology.

X-Ray Diffraction (XRD) HAp-Urea nanofertilizers

XRD in the interval of angles 20° ≤ (2θ) ≤ 60° (Cu Kα radiation; Bruker Advanced X-ray Solution D8, Bremen, Germany) was used to determine the lattice parameter, crystallite size, and phase of powders. The X'Pert High Score Plus software was used. Inferred patterns were matched with the International Center for Diffraction Data with file number 00-009-0432 designated for standard HA to estimate the phase type and size of crystals. The crystallite size was calculated by XRD through Scherrer's equation (Eq. (4.0)) (Wagoner Johnson and Herschler, 2011):

$$D_{scherrer} = \frac{K\lambda}{\beta \frac{1}{2} \cos\theta} \quad (4)$$

Where $D_{scherrer}$ refers to the crystallite size (nm), λ (1.5404 Å) refers to the wavelength of Cu Kα radiate on, β) refers to the full width at half maximum (radian), θ is the diffraction angle (degrees), and k is the boarding constant (0.94). In this regard, distinct diffraction peaks of (002), (211), and (300) with high intensities, were selected for evaluation. Rietveld refinement was conducted on the chemical compound to confirm the effect of ions on the apatite structure.

X-Ray Fluorescence (XRF) of HAp-Urea nanofertilizers

Emission of specific atomic energies of different elements permits an XRF spectrometer to analyze which elements are present in any given composition; the number of

energies detected supply quantitative information (West, 2013). In this study, powders of each the CHAp samples were mixed each with a flux in a platinum crucible, heated to 1050 ˚C to form a glass bead. The various glass beads were used to quantify the atomic concentration of elements of various samples by XRF spectrometer (Rix 3000; Rigaku, Tokyo, Japan).

Fourier Transform Infra-Red (FTIR) Spectroscopy of HAp-Urea nanofertilizers

Infrared spectroscopy investigates the molecular vibrations by matching the unique infrared wave bands of a functional group with the vibrations of the functional groups. (Berthomieu and Hienerwadel, 2009). The types of bonding and chemical distinctiveness were determined by FTIR (Spectrum One; Perkin-Elmer, Waltham, MA, USA) in the 400–4000 cm^{-1} range with the help of the Spectrum software. 0.4 to 1.0 mg of each composition was mixed with 200 to 400 mg of KBr, manually milled and pressed with a force of 28 MPa for 2 minutes into a translucent wafer. Finally, the compact pellet was transferred into the machine and then probed in a transmittance mode.

Field Emission Scanning Electron Microscopy (FE-SEM) HAp-Urea nanofertilizers

FE-SEM operation was achieved by the liberation and acceleration of high-energy beam of electrons in a raster scan pattern from field emission gun sources. In this study, the morphology of the powder surfaces of HU, HUMS and HUMSC were examined by FE-SEM (S35VP; Zeiss, Dublin, CA, USA). In addition, the formations of apatite layer on all sintered pellets immersed in SBF solution were analyzed using FE-SEM. The samples were prepared by sputtering of gold film on samples to form a surface coat. The surface coat ensured effective surface conductivity of the samples that prevents image defects.

Transmission Electron Microscopy (TEM)

The variation of TEM micrograph depends on wave scattering and interference that create variant mass, thickness, diffraction, atomic-number (*Z*), and phase (Cross et al., 2015). The TEM specimens were prepared so that the electron beam can penetrate the area to be analyzed. The sample preparation was conducted by dispersing particles into acetone solution followed by 15 minutes of ultrasonication. Then mixed samples were careful dropped on a copper grid and observed using Philip CM12 TEM. The Image J™ software was used to ascertain the particle size of the powders, as determined by TEM.

2.2.6 Specific Surface Area (SSA) of HAp-Urea nanofertilizers

The absorbed of nitrogen at numerous partial pressures in BET is quantified and used to plot an isotherm. The shape of the isotherm revealed vital surface and pore size and distribution information.

Total surface area = (Number of adsorbed gas molecules) × (Area/molecule) (5)

The BET method accounts for the formation of multiple layers adsorbed to a substrate surface.

$$1W\left[(P_o/P_i) - 1\right] = 1WmC + (C-1)\,WmCPiPo \quad (6)$$

Where *W*; weight of the nitrogen adsorbed at a given P_i/P_o and *Wm*; weight of the gas to give monolayer coverage and *C*; constant that is related to the heat of adsorption. The direct relationship between $1/W/\left[(P_o/P_i) - 1\right]$ and P_i/P_o is needed to deliver the amount of the nitrogen adsorbed. At this region of the isotherm, P_i/P_o = 0.05–0.3 and formed the multi-layer adsorption on the substrate (Collins, 2012). Parameters used in this study include nitrogen adsorption–desorption conducted at approximately 150 °C during the measurement of the BET surface area. Also, the measured volume of gas (N_2) adsorbed at a given pressure for the compositions was conducted after applying liquid nitrogen as coolant. The resultant isotherm adsorption link at P_i/P_o = 0.95 generated the pore volume. A derived BET surface area particle size was assessed using the formula:

$$P_{S_{\mathrm{BET}}} = \frac{6,000}{S_{\mathrm{BET}} \cdot \rho}, \quad (7)$$

Where $P_{S_{\mathrm{BET}}}$ is the BET particle size, S_{BET} is the surface area, and ρ is the theoretical density.

Micronutrient Ion Release of HAp-Urea nanofertilizers

HAp-Urea nanofertilizers ion release was ascertain after 14 days in water and liquid media, respectively. For the water medium, a ratio of 12.5 mg/ml powder to water solution will used. The concentration of Ca^{2+} and PO_4^{3-} ions in the leachate of the water medium was quantified by Inductive Coupled Plasma Optical Emission Spectroscopy (ICP-OES: Perkin Elmer Optima 7300 DV, USA). The leachate was converted into a vapor of fine aerosol which allowed for transportation via a nebulizer with an argon stream into a plasmatic burner. Determination of the concentrations of ion release for Ca^{2+}; 393.366, P^{5+}; 177.499, Mg^{2+}; 279.553 and Cu^{2+}; 324.754 nm was measured at the given wavelength. For the soil ion release test, soil samples containing HAp-Urea nanofertilizers was collected after 14 days and analyze using ICP-OES.

Plant Foliage Analysis HAp-Urea nanofertilizers

This will involves activities such as the treatment of plant

Table 2: Structural features, BET specific surface area and derived particle size of the HU, HUMS and HUMSC nanoparticles.

Sample	Lattice constant			$D_{Scherer}$	Lattice	FWHM	X_C%	SA_{BET}	P_{SBET}	d_{TEM}
	a (Å)	*c* (Å)	*c*/*a*	(nm) [x]	(ε)(%) [y]	(º)	(%) [z]	(m^2g^{-1})	(nm)	(nm)
HU	9.42	6.88	0.73	34.68	0.33	0.25	97.96	77.30	31.48	29.87
HUMS	9.42	6.88	0.73	23.60	0.47	0.36	66.67	176.70	16.40	15.47
HUMSC	9.39	6.85	0.73	22.75	0.52	0.39	61.53	157.84	17.80	19.40

Table 3: XRF analysis of compositions and Ca/P ratios of all the as-synthesized powders

Sample	Elemental Compositions (wt. %)						
	Mg^{2+}	Si^{4+}	Cu^{2+}	Ca^{2+}	P^{5+}	O^{2-}	[Ca/P]
HU	-	-	-	23.9727	02.6665	63.3608	1.89
HUMS	0.2533	0.0269	-	21.2742	11.5674	66.8783	1.84
HUMSC	0.2361	0.0667	0.0065	20.0110	10.8646	68.8151	1.84

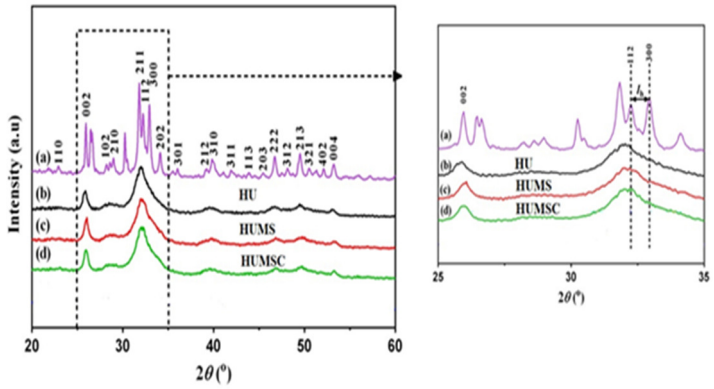

Figure 1: Phase features of nanoparticles: (left) XRD patterns of (a) Standard HAp (b) HU (c) HUMS (d) HUMSC; (right) enlarged XRD patterns at 2*θ*: 25–35˚ with peak shift at (200) and (300) and crystalline phase by intensity of hollow (I_h) between (112) and (300) reflections.

with 10g of synthesized HAp-Urea nanofertilizers in relation to 10g of commercial fertilizer in a specified duration. A plant of height and foliage yield activities was taken after 30 days. The plant for this study is chilly pepper extracted from fresh ripped fruit bud and planted in a loamy soil collected from Auchi, Edo state.

Statistical analysis

The results of the experiments are represented as mean and arithmetic standard deviation (±S.D.) for m=4. The one-way ANOVA test with a significance level of ($p^*<0.05$) using GraphPad Prism software (Version 6.) was used for the statistical analysis of the experiment.

RESULTS AND DISCUSSION

The multidoped HAp-Urea nanofertilizers samples are estimated to uphold amorphous structure with particle sizes in the nanometres. The synthesized HAp-Urea nanofertilizer is expected to possess overall improved flora performance in contrast to commercial fertilizer.

X-Ray Diffraction (XRD) HAp-Urea nanofertilizers

XRD patterns of the synthesized HU, HUMS and HUMSC in comparison to standard HAp (Sigma-Aldrich) is shown in (Figure 1). An enlarged pattern at 25° ≤ (2*θ*) ≤ 35°, indicated a shift of peaks reflections around (002) and (300) in HU. This shift was visible in HU compared with the reference standard HAp peak due to the relatively crystalline pattern caused by lower CO_3^{2-}/PO_4^{3-} molar ratio. However, HUMS and HUMSC reveal various amorphous phase structures due increased dopant activities in the Ca^{2+} and PO_4^{3-} locations respectively (Furko et al., 2018). The shift in peaks was due to strain from planar stress in apatite structure due to CO_3^{2-} substitution and complied with Bragg's law $2d_{hkl}Sin\theta_{hkl} = n\lambda$ where such diffraction depends on the size of the substituent species as reported by (Venkateswarlu et al., 2014). In Table 2, the most inhibited pattern as reflected in the lowest crystallite size was observed in HUMS with $d_{Scherer}$, 3.27 nm. Magnesium and carbonate incorporation, individually or in combination, was reported to have the disposition of inducing low crystallinity and increase in structural defects within the apatite lattice (Sader et al., 2013).

X-Ray Fluorescence (XRF) of HAp-Urea nanofertilizers

XRF was employed in the determination the Ca/P ratio of

HU, HUMS and HUMSC samples as shown in (Table 3). The elemental analysis shows a fairly close composition and stoichiometry consistent with apatite composition. In general, the difference in values compared with the theoretical estimation was recorded across most of the elements. Such lower dopant content of the corresponding amount of starting material implied that some of such ions remain in the mother liquor solution after preparation by method such as wet chemical route as suggested by (Kim et al., 2004).

Fourier Transform Infra-Red (FTIR) Spectroscopy of HAp-Urea nanofertilizers

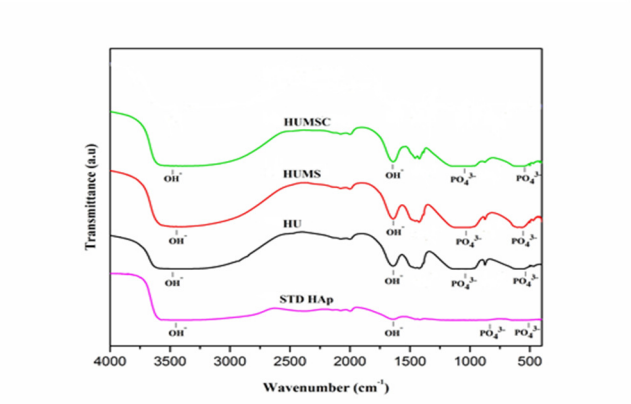

Figure 2: FTIR spectra of standard HAp, HU, HUMS and HUMSC nanoparticles.

FTIR outcomes of the nanoparticles of HU, HUMS and HUMSC are shown in (Figure 2). Sample HU was devoid of PO_4^{3-} spectral band at v_2 bending mode 878-888cm^{-1} reported as an indicator (Fleet, 2009). Interestingly, the broad band around 1600-1700 and 3200-3600 cm^{-1} in all the prepareded samples have been attributed to the presence of absorbed water in similar study reported elsewhere (Li et al., 2017).

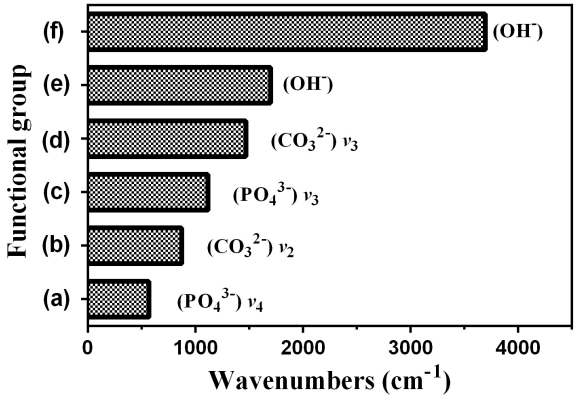

Figure 3: Functional groups' and equivalent wavenumber from FTIR analysis (a) †550-570(Li et al., 2017) (b) ‡870-875 (Meejoo et al., 2006) (c) 1020-1120 (Destainville et al., 2003) (d) ‡1450-1470 (e) 1600-1700 (f) †3200-3600 cm^{-1}

Furthermore, the HU exhibited a similar band positions and ranges of the functional groups OH^-, PO_4^{3-}, and CO_3^{2-} associated with standard HAp. A depiction of FTIR characteristics of the as-synthesized nanoparticles as discuss above are consistent with established research as shown in (Figure 3).

FESEM of HAp-Urea nanofertilizers

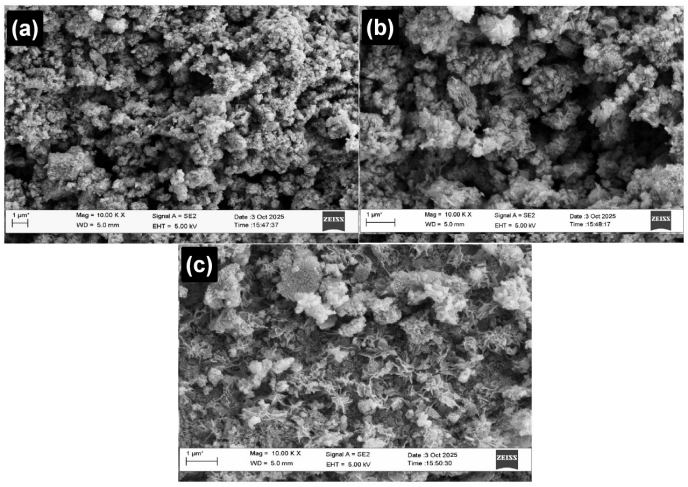

Figure 4: FESEM micrographs of nanoparticles (a) HU (b) HUMS (c) HUMSC.

The FESEM micrographs were used to characterize the morphology of the as-synthesized HU, HUMS and HUMSC nanoparticles. The micrographs displayed in (Figures 4a-c), for all samples revealed similar agglomerated morphology consistent with nanoparticles. Such agglomerations as observed are as a result from a strong interparticle attraction between the nanoparticles after in situ formation (Liou et al., 2005).

Transmission Electron Microscopy (TEM) of HAp-Urea nanofertilizers

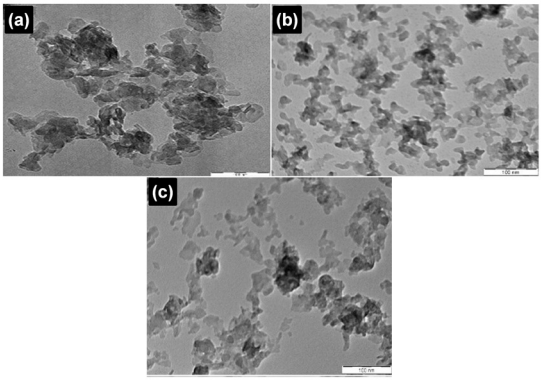

Figure 5: TEM micrographs of nanoparticles (a) HU (b) HUMS (c) HUMSC.

The TEM micrographs in (Figure 5) showed HU, HUMS and HUMSC nanoparticles having spherical crystals likely

linked to crystalline HAp prepared via wet method (Sadat-Shojai et al., 2013). In (Table 2), the TEM particle sizes (d_{TEM}) in all samples exhibited sizes in the nanometric region consistent with other nanomaterials reported elsewhere (Li and Pasteris, 2014, Kon et al., 2014). The measured d_{TEM} and P_{SBET} nanoparticle showed lowest diminutive size for HUMS sample at 15.47 nm with the largest BET specific surface area 176.70 m^2g^{-1}. Conversely, the largest nanoparticle size was found in HU at 29.87 nm (with SA_{BET} at 77.30 m^2g^{-1}) and HUMSC at 19.40 nm (with SA_{BET} at 157.84 m^2g^{-1}).

Micronutrient Ion Release of HAp-Urea nanofertilizers

The ion release when the HUMSC nanoparticle was

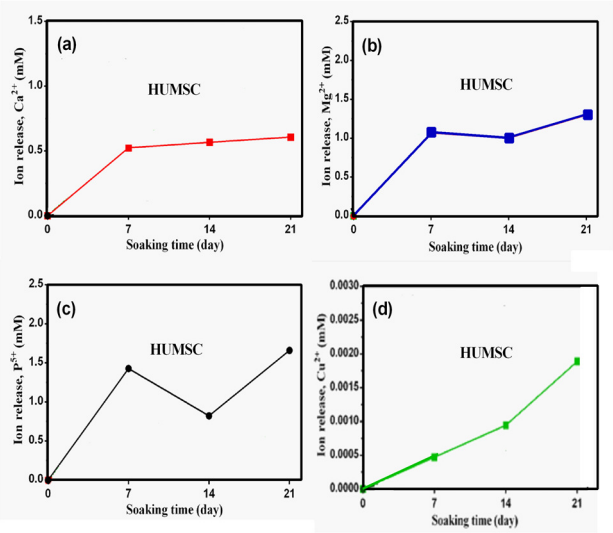

Figure 6: Micronutrient ion release for HUMSC sample (a) Ca^{2+} (b) Mg^{2+} (c) P^{5+} (d) Cu^{2+}.

immersed in soil fluid solution was also analyzed for Ca^{2+}, Mg^{2+}, P^{5+} and Cu^{2+} release. In Figure 6, the ion release in soil fluid solution for all samples increased with soaking duration of 7days indicates inherent dissolution ability. Figure 6(a), the Ca^{2+} ion release increased upwardly 0.5 mM for day 7, 0.52 mM for day 14 and 0.54 mM for day 21, respectively.

In Figure 6(b), the Mg^{2+} ion release in soil fluid solution for HUMSC samples showed that Mg^{2+} ion release increased after day 7 to 1.2 mM a day 7, which slightly decreased to 1.0 mM after day 14 and surged to 1.3 mM after day 21, respectively. In Fig. 6(c), the P^{5+} ion release in soil fluid solution for HUMSC samples displayed that P^{5+} ion release increased after day 7 to 1.5 mM a day 7, which significantly decreased to 0.57 mM after day 14 and significantly surge to 1.52 mM after day 21, respectively.

Finally, Figure 6(d), the Cu^{2+} ion release in soil fluid solution for HUMSC samples demonstrated that Cu^{2+} ion release increased marginally after day 7 to 0.0004 mM a day 7, which continued significantly to 0.0009 mM after day 14 and doubled to 0.0018 mM after day 21, respectively.

Plant Height and Foliage Analysis of HAp-Urea nanofertilizers

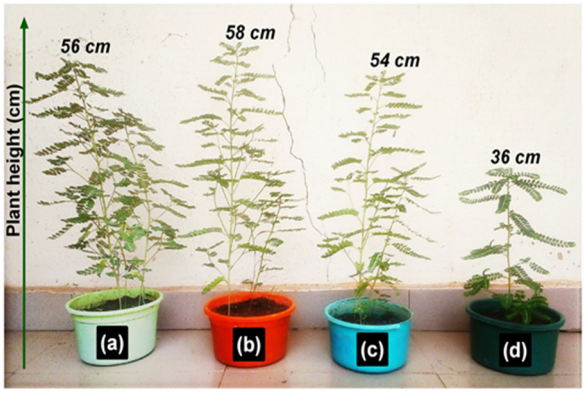

Figure 7: Plant height after 30 days with (a) HUMSC (b) HUMS (c) HU (d) Commercial fertilizer.

The plant height is shown in Figure 7 with commercial fertilizer, HU, HUMS and HUMSC samples each applied chili pepper. The effect of these samples on plant height in comparison with commercial fertilizer demonstrated remarkable differences. After 30 days HU, HUMS and HUMSC nanoparticles applied on various plant displayed significant growth higher than the commercial fertilizer sample. The result revealed significant growth height for HU at 54 cm (Figure 7(a)), HUMS at 58 cm (Figure 7(b)) and HUMSC (Figure 7(c)) at 56 cm while the commercial fertilizer sample stood at 36 cm (Fig. 7(d)). A study indicated that the combination of organic and mineral fertilizers can significantly increase growth. The report further stated that to achieve the ideal saturation levels, Ca, Mg, and K fertilizers should be applied in appropriate amounts based on the results of the soil analysis (Yan, Zhou, Hang, Chen, Liu, Su, Lv, Jia and Zhao, 2024). The increased growth in HU, HUMS and HUMSC can be attributed to the critical roles calcium Ca^{2+}, phosphorus (P^{5+}), Si^{4+} and magnesium (Mg^{2+}) play not only in plant structure and physiology but also in influencing the uptake of other essential nutrients.

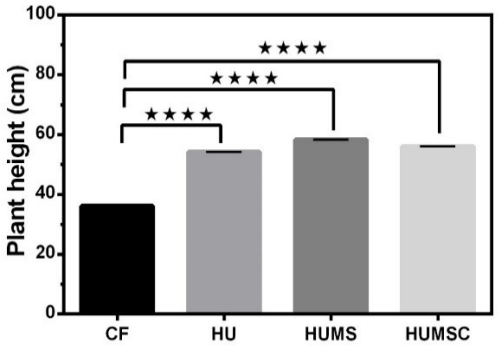

Figure 8: One way ANOVA of plant growth height of HU, HUMS and HUMSC in comparison with CF (*P < 0.0001).

In Figure 8, ANOVA was conducted to compare the effect

of commercial fertilizer (CF), HU ($[Ca_{10}(PO_4)_6(OH)_{2.00}]$ + Urea), HUMS ($[Ca_{9.220}Mg_{0.760}(PO_4)_{5.922}(SiO_4)_{0.0371}(OH)_{1.963}]_+$ + Urea) and HUMSC ($[Ca_{9.220}Mg_{0.760}Cu_{0.0001}(PO_4)_{5.923}(SiO_4)_{0.0371}(OH)_{1.963}]$ + Urea) on chili plant. Comparisons in terms of plant growth height in cm after 30 days were made among CF vs. HU, CF vs. HUiMS and CF vs. HUMSC groups. There was a significant difference among the types of nanocomposite samples and the commercial fertilizer at *P < 0.0001 level for the three groups F (3, 8) = 1.545e+006. Dunnett's multiple comparisons test results revealed that CF vs. HU group had significantly lower mean difference (M = 18.04, SD = 0.01155) compared to the intense CF vs. HUMS (M = 22.12, SD = 0.01155).

Conclusion

Nanofertilizers are one of the most promising solutions or substitutes for conventional fertilizers. These engineered materials are composed of nanoparticles containing macro- and micronutrients that are delivered to the plant rhizosphere in a regulated manner. In nanofertilizers, the essential minerals and nutrients (such as N, P, K, Fe, and Mn) are bonded alone or in combination with nano-dimensional adsorbents. The study combined multidoped HAp prepared using wet chemical route and made into composite with nano-urea composite in an ultrasound sonication setup. Ionic species such as Mg^{2+}, Si^{4+} and Cu^{2+} in the hexagonal calcium phosphate (CaP) apatite structure served as additional nutrient bases of the synthesized nanofertilizer. XRD (34.68, 23.60 and 22.75 nm), TEM (29.87, 15.47 and 19.40 nm) and BET (31.48, 16.40 and 17.80 nm) analysis corroborated the nanoparticle properties of HU, HUMS and HUMSC. Comparatively, HU, HUMS and HUMSC nanofertilizer displayed better growth height and foliage features to the commercial fertilizer hence have potentials for chili production with higher yield. When compared to conventional fertilizer, which had a PGH of 36 cm, the multidoped HAp-urea composite-based nanofertilizer demonstrated superior plant growth height (PGH) of HU: 54, HUMS: 58, and HUMSC: 56 cm.

Conflict of Interests

The author declares that there is no conflict of interests regarding the publication of this paper

Acknowledgments

The authors sincerely acknowledge the financial support provided by Tertiary Education Trust Fund, TETF/DR&D/CE/POL/AUCHI/IBR/2025/VOL.1

REFERENCES

Abeywardana, L., de Silva, M., Sandaruwan, C., Dahanayake, D., Priyadarshana, D., Chathurika, S., Karunaratne, V., & Kottegoda, N. (2021). Zinc-doped hydroxyapatite–urea nanoseed coating as an efficient macro–micro plant nutrient delivery agent. ACS Agricultural Science & Technology, 1(3), 230–239.

Ammar, M., Ashraf, S., & Baltrusaitis, J. (2023). Nutrient-doped hydroxyapatite: Structure, synthesis and properties. Ceramics, 6(3), 1799–1825.

Ashraf, U., Batool, F., Ghaffar, R., Imran, M., Riaz, A., Hussaan, M., Farooq, M. A., & Rasul, F. (2025). Nanomaterials as nanofertilizers for climate-smart agriculture. https://doi.org/10.1007/978-981-96-4499-5_15

Ayushi, P., Ratul, K. D., Aaron, S., & Pushplata, P. S. (2019). A new method for biological synthesis of agriculturally relevant nanohydroxyapatite with elucidated effects on soil bacteria. Scientific Reports, 9, 15083. https://doi.org/10.1038/s41598-019-51514-0

Aziz, A., Majid, M., Peters, E., Amanullah, M., Md, A. H., Hafeez, A. T., Sirilak, C., Khalid, U. S., Habibullah, A., & Shakeel, A. T. (2026). Climate-smart agriculture as disaster risk reduction: Effectiveness varies by hazard type in Pakistan. Climate Smart Agriculture, 3(1), 100093. https://doi.org/10.1016/j.csag.2025.100093

Baijukya, F. P., Van H. J., Franke, A. C., Van den B. G. J., Foli, S., K. L., Seitz, T., Servan, L., Vanlauwe, B., & Giller, K. E. (2021). Nutrient deficiencies are key constraints to grain legume productivity on "non-responsive" soils in Sub-Saharan Africa. Frontiers in Sustainable Food Systems, 5, 678955. https://doi.org/10.3389/fsufs.2021.678955

Berthomieu, C., & Hienerwadel, R. (2009). Fourier transform infrared (FTIR) spectroscopy. Photosynthesis Research, 101, 157–170.

Carmona, F. J., Dal Sasso, G., Ramírez-Rodríguez, G. B., Pii, Y., Delgado-López, J. M., Guagliardi, A., & Masciocchi, A. (2021). Urea functionalized amorphous calcium phosphate nanofertilizers: Optimizing the synthetic strategy towards environmental sustainability and manufacturing costs. Scientific Reports, 11, 1419.

Carmona, F. J., Guagliardi, A., & Masciocchi, N. (2022). Nanosized calcium phosphates as novel macronutrient nano fertilizers. Nanomaterials, 12(15), 2709.

Collins, A. M. (2012). Chapter 3 - Common analytical techniques for nanoscale materials. In Nanotechnology Cookbook (pp. xx–xx). Elsevier.

Cross, J. O., Opila, R. L., Boyd, I. W., & Kaufmann, E. N. (2015). Materials characterization and the evolution of materials. MRS Bulletin, 40, 1019–1034.

Dawar, N., Chitkara, M., Sandhu, I. S., Jolly, J. S., & Malhotra, S. (2016). Structural, magnetic and dielectric properties of pure and nickel-doped barium nanohexaferrites synthesized using chemical co-precipitation technique. Cogent Physics, 3(1). https://doi.org/10.1080/23311940.2016.1208450

Elhassani, C. E., Essamlali, Y., Aqlil, M., Nzenguet, A. M., Ganetri, I., & Zahouily, M. (2019). Urea-impregnated HAP encapsulated by lignocellulosic biomass-extruded composites: A novel slow-release fertilizer. Environmental Technology & Innovation, 15, 100403.

Elshay, O. M., Nada, A. M., Farroh, K. Y., AL-Huqail, A. A., Aljabri, M., Binothman, N., & Seleiman, M. F. (2022). Utilizing urea–chitosan nanohybrid for minimizing synthetic urea application and maximizing Oryza sativa L. productivity and N uptake. Agriculture, 12(7), 944.

Fernan Ramírez-Rodríguez, G. B., Miguel-Rojas, C., Montanha, G. S., Carmona, F. J., Dal Sasso, G., Sillero, J. C., Skov Pedersen, J., Masciocchi, N., Guagliardi, A., & Pérez-de-Luque, A. (2020). Reducing nitrogen dosage in Triticum durum plants with urea-doped nanofertilizers. Nanomaterials, 10(6), 1043.

Fernando, N. F., Rathnayake, D. T., Kottegoda, N., Jayanetti, J. S., Karunaratne, V., & Jayasundara, D. R. (2021). Mechanistic insights into interactions at urea–hydroxyapatite nanoparticle interface. Langmuir, 37(22), 6691–6701.

Fihri, A., Len, C., Varma, R. S., & Solhy, A. (2017). Hydroxyapatite: A review of syntheses, structure and applications in heterogeneous catalysis. Coordination Chemistry Reviews, 347, 48–76.

Fleet, M. E. (2009). Infrared spectra of carbonate apatites: v2-region bands. Biomaterials, 30, 1473–1481.

Fuad, N. A. S. M., Ang, L. S., Nabil, N. N. A. M., & Shuhaime, N. (2023). Theoretical investigations on the interactions of urea with hydroxyl and Non-hydroxyl hydroxyapatite. Surface, 20(6), 6558.

Furko, M., Havasi, V., Kónya, Z., Grünewald, A., Detsch, R., Boccaccini, A. R., & Balázsi, C. (2018). Development and characterization of multi-

element doped hydroxyapatite bioceramic coatings on metallic implants for orthopedic applications. Boletín de la Sociedad Española de Cerámica y Vidrio, 57, 55–65.

Imran, & Hayat, Z. (2025). Application of nano fertilizers and climate-smart agriculture practices for sustainable soil, water, and environmental management. Communications in Soil Science and Plant Analysis. https://doi.org/10.1080/00103624.2025.2577399

Kabato, W., Getnet, G. T., Sinore, T., Nemeth, A., & Molnár, Z. (2025). Towards climate-smart agriculture: Strategies for sustainable agricultural production, food security, and greenhouse gas reduction. Agronomy,15(3), 565. https://doi.org/10.3390/agronomy15030565

Kim, H. M., Himeno, T., Kawashita, M., Kokubo, T., & Nakamura, T. (2004). The mechanism of biomineralization of bone-like apatite on synthetic hydroxyapatite: An in vitro assessment. Journal of The Royal Society Interface, 1, 17–22.

Kottegoda, N., Sandaruwan, C., Priyadarshana, G., Siriwardhana, A., Rathnayake, U. A., Arachchige, D. B. M., Kumarasinghe, A. R., Dahanayake, D., Karunaratne, V., & Amaratunga, G. A. (2017). Urea-hydroxyapatite nanohybrids for slow release of nitrogen. ACS Nano, 11(2), 1214–1221.

Li, D., Huang, X., Wu, Y., Li, J., Cheng, W., He, J., Tian, H., & Huang, Y. (2016). Preparation of pH-responsive mesoporous hydroxyapatite nanoparticles for intracellular controlled release of an anticancer drug. Biomaterial Science, 4(2), 272–280.

Li, R., Zhu, G., Chen, X. L., Qi, S., Lu, M., & Gun, Y. (2025). Global stable isotope dataset for surface water. Earth System Science Data, 17(5), 2135–2145. https://doi.org/10.5194/essd-17-2135-2025

Liou, S. C., Chen, S. Y., & Liu, D. M. (2005). Manipulation of nanoneedle and nanosphere apatite/poly(acrylic acid) nanocomposites. Journal of Biomedical Materials Research Part B: Applied Biomaterials, 73, 117–122.

Liu, X., Ruan, Y., Li, C., & Cheng, R. (2017). Effect and mechanism of phosphoric acid in the apatite/dolomite flotation system. International Journal of Mineral Processing, 167, 95–102.

Lubkowski, K. (2016). Environmental impact of fertilizer use and slow release of mineral nutrients as a response to this challenge. Polish Journal of Chemical Technology, 18, 72–79.

Madusanka, N., Sandaruwan, C., Kottegoda, N., Sirisena, D., Munaweera, I., De Alwis, I., Karunaratne, V., & Amaratunga, G. (2017). Urea–hydroxyapatite-montmorillonite nanohybrid composites as slow release nitrogen compositions. Applied Clay Science, 150, 303–308.

Maghsoodi, M. R., Najaf, A., Reyhanitabar, A., & Oustan, N. (2020). Hydroxyapatite nanorods, hydrochar, biochar, and zeolite for controlled-release urea fertilizers. Geoderma, 379, 114644.

Noruzi, M., Hadian, P., Soleimanpour, L., Ma'mani, L., & Shahbazi, L. (2023). [Title missing]. Chemical Biology Technologies in Agriculture, 10, 71. https://doi.org/10.1186/s40538-023-00437-0

Pohshna, C., & Mailapalli, D. R. (2021). Engineered urea-doped hydroxyapatite nanomaterials as nitrogen and phosphorus fertilizers for rice. ACS Agricultural Science & Technology, 2(1), 100–112.

Rao, C. Y., Sun, X. Y., & Ouyang, J. M. (2019). Effects of physical properties of nano-sized hydroxyapatite crystals on cellular toxicity in renal epithelial cells. Materials Science and Engineering: C, 103, 109807.

Sadat-Shojai, M., Khorasani, M.-T., Dinpanah-Khoshdargi, E., & Jamshidi, A. (2013). Synthesis methods for nanosized hydroxyapatite with diverse structures. Acta Biomaterialia, 9, 7591–7621.

Sajadinia, H., Ghazanfari, D., Naghavii, K., Naghavi, H., & Tahamipur, B. (2021). A comparison of microwave and ultrasound routes to prepare nano-hydroxyapatite fertilizer improving morphological and physiological properties of maize (Zea mays L.). Heliyon, 7(3), e060941.

Samadi, A., Pourmadadi, M., Yazdian, F., Rashedi, H., & Navaei-Nigjeh, A. (2021). Ameliorating quercetin constraints in cancer therapy with pH-responsive agarose polyvinylpyrrolidone-hydroxyapatite nanocomposite encapsulated in double nanoemulsion. International Journal of Biological Macromolecules, 182, 11–25.

Sharma, B., Shrivastava, M., Afonso, L. O., Soni, U., & Cahill, D. M. (2022). Zinc- and magnesium-doped hydroxyapatite nanoparticles modified with urea as smart nitrogen fertilizers. ACS Applied Nano Materials, 5(5), 7288–7299.

Siracusa, V., Maimone, G., & Antonelli, V. (2021). State-of-art of standard and innovative materials used in cranioplasty. Polymers, 13(9), 1452.

Tarafder, C., Morshed, A., Ripon, A., Jahidul, I., Rakibul, Sohel, I., Mohamedm, A., & Zaved, H. A. (2020). Formulation of a hybrid nanofertilizer for slow and sustainable release of micronutrients. ACS Omega, 5, 23960–23966. https://doi.org/10.1021/acsomega.0c03233

Thathsarani, M. (2021). Nanofertilizer for precision and sustainable agriculture. Journal of Research in Technology Engineering, 2(1), 81–85.

Ullah, R., Sher, S., Muhammad, Z., Jan, S. A., & Nafees, M. (2022). Modulating response of sunflower (Helianthus annuus) to induced salinity stress through application of engineered urea functionalized hydroxyapatite nanoparticles. Microscopy Research and Technique, 85(1), 244–252.

Usman, M., Farooq, M., Wakeel, A., Nawaz, A., Cheema, S. A., Rehman, H., Ashraf, I., & Sanaullah, M. (2020). Nanotechnology in agriculture: current status, challenges and future opportunities. Science of the Total Environment, 721, 137778.

Wagoner Johnson, A. J., & Herschler, B. A. (2011). A review of the mechanical behavior of CaP and CaP/polymer composites for applications in bone replacement and repair. Acta Biomaterialia, 7, 16–30.

Venkateswarlu, K., Sandhyarani, M., Nellaippan, T. A., & Rameshbabu, N. (2014). Estimation of crystallite size, lattice strain and dislocation density of nanocrystalline carbonate substituted hydroxyapatite by X-ray peak variance analysis. Procedia Materials Science, 5, 212–221.

Wang, D., Jin, Y., & Jaisi, P. D. (2015). Effect of size-selective retention on the cotransport of hydroxyapatite and goethite nanoparticles in saturated porous media. Environmental Science & Technology, 49(14), 8461–8470.

Wei, Z., Kou, J., Miao, L., Hu, F., Li, L., Wu, X., & Meng, L. (2025). Exploring diurnal variation in soil moisture via sub-daily estimates reconstruction. Journal of Hydrology, 662, 134005. https://doi.org/10.1016/j.jhydrol.2025.134005

West, M. (2013). X-ray fluorescence spectrometry and related techniques: An introduction. Momentum Press.

Wu, X., & Zhao, Y. (2024). A novel heat pulse method in determining "effective" thermal properties in frozen soil. Water Resources Research,60(12),e2024WR037537.https://doi.org/10.1029/2024WR037537

Yang, M., Zhou, D., Hang, H., Chen, S., Liu, H., Su, J., Lv, H., Jia, H., & Zhao, G. (2024). Effects of balancing exchangeable cations Ca, Mg, and K on the growth of tomato seedlings (Solanum lycopersicum L.) based on increased soil cation exchange capacity. Agronomy, 14(3), 629. https://doi.org/10.3390/agronomy14030629

Zhang, Y., & Wu, X. (2025). Global space-time patterns of sub-daily extreme precipitation and its relationship with temperature and wind speed. Environmental Research Letters, 20(8), 084019.https://doi.org/10.1088/1748-9326/ade607